

000  
001  
002054  
055  
056

# Multi-channel Weighted Nuclear Norm Minimization for Real Color Image Denoising

057  
058  
059003  
004  
005  
006  
007060  
061  
062  
063

Anonymous ICCV submission

008  
009  
010  
011  
012064  
065  
066  
067  
068

Paper ID 572

013  
014  
015069  
070  
071

## Abstract

016  
017  
018  
019  
020072  
073  
074  
075  
076

The noise structures among the R, G, B channels of real images are quite different due to the preprocessing steps, such as demosaicing, white balance, etc., of the in-camera imaging pipelines. This makes the real image denoising problem much more complex than traditional grayscale image denoising. In this paper, we propose a multi-channel optimization model for real color image denoising. Specifically, we introduce a weighting matrix into the data term to process adaptively each part of R, G, B channels in the joint patches concatenated by corresponding patches in these channels. In the regularization term, we employ the weighted nuclear norm to exploit the non-local self similar property. The proposed multi-channel weighted nuclear norm minimization (WNNM) model is much more complex than the standard WNNM model. We reformulate the proposed model into a linear constrained optimization problem and solve it by the alternating direction method of multipliers algorithm. Each alternative updating step has closed-form solution and the convergence results are given. Experiments on benchmark datasets demonstrate that the proposed model outperforms state-of-the-art denoising methods on synthetic as well as real-world noisy images.

038  
039  
040  
041077  
078  
079  
080

## 1. Introduction

042  
043  
044  
045  
046081  
082  
083  
084  
085

Image denoising is an important problem in enhancing the image quality in computer vision systems. The traditional grayscale image denoising problem aims to recover the clean image  $\mathbf{x}$  from the noisy observation  $\mathbf{y} = \mathbf{x} + \mathbf{n}$ , where  $\mathbf{n}$  is often assumed to be additive white Gaussian noise (AWGN). Most image denoising methods in this field either employ the non-local self similarity (NSS) of natural images [1–7] or learn generative or discriminative denoisers from paired natural clean images and synthetic noisy images [8–12]. Among these methods, the weighted nuclear norm minimization (WNNM) method achieves excellent denoising performance by exploiting the NSS property

via low rank regularization.

The real color image denoising problem is not a trivial extension from single channel (grayscale image) to multiple channels (color image). The reason is that the noise structures are quite different among the R, G, B channels of images captured by CCD or CMOS cameras due to the on-board processing steps [13]. This makes the real color image denoising problem much more complex. Directly applying the denoising methods for grayscale images to each channel of color images separately would obtain bad performance [14]. There are several work [14–19] proposed specifically for color image denoising. The method [15] first transforms the color images into the luminance/chrominance space such as YCbCr before denoising, but this would make the noise distribution more complex in color images. The methods of [14, 19] process the joint patches concatenated by the corresponding patches in R, G, B channels and treat equally the patches in different channels. This would generate false colors or artifacts [14]. The methods of [16–18] ignore the non-local self similarity property of natural images, and their performance would be largely depressed [2, 7].

In order to deal with the R, G, B channels in color images more effectively, different noise properties of different channels should be considered in solving real color image denoising problem. Besides, due to its expressive denoising performance, the WNNM model [7] is employed to exploit the NSS property of natural images. In this paper, we proposed a multi-channel WNNM model for real color image denoising. By introducing a weighting matrix to the WNNM model, the proposed multi-channel WNNM model no longer has closed-form solutions and more challenging to solve. By reformulating the proposed multi-channel WNNM model into a linear constrained program with two variables, the relaxed problem can be solved under the alternating direction method of multipliers (ADMM) [20] framework. Each variable can be updated with closed-form solution [7, 21]. We also give the convergency results with detailed proof to guarantee a rational termination of the proposed algorithm.

108

## 2. Related Work

109

### 2.1. Weighted Nuclear Norm Minimization

111

As an extension to the nuclear norm minimization (NNM) model [22], the weighted nuclear norm minimization (WNNM) model [7] is described as

$$\min_{\mathbf{X}} \|\mathbf{Y} - \mathbf{X}\|_F^2 + \|\mathbf{X}\|_{w,*} \quad (1)$$

115

where  $\|\mathbf{X}\|_{w,*} = \sum_i w_i \sigma_i(\mathbf{X})$  is the weighted nuclear norm of matrix  $\mathbf{X}$ , and  $w = [w_1, \dots, w_n]^\top$ ,  $w_i \geq 0$  is the weight vector,  $\sigma_i(\mathbf{X})$  is the  $i$ -th singular value of matrix  $\mathbf{X}$ . According to the Corollary 1 of [23], the problem (1) has closed-form solution if the weights are non-decreasing

$$\hat{\mathbf{X}} = \mathbf{U} \mathcal{S}_{w/2}(\Sigma) \mathbf{V}^\top \quad (2)$$

121

where  $\mathbf{Y} = \mathbf{U} \Sigma \mathbf{V}^\top$  is the singular value decomposition [24] of  $\mathbf{Y}$  and  $\mathcal{S}_\tau(\bullet)$  is the generalized soft-thresholding operator with weight vector  $w$ :

$$\mathcal{S}_{w/2}(\Sigma_{ii}) = \max(\Sigma_{ii} - w_{ii}/2, 0) \quad (3)$$

125

Though having achieved excellent performance on grayscale image denoising, the WNNM model would generate false colors or artifacts [14], if being directly extended to real color image denoising by processing each channel separately or joint vectors concatenated by multiple channels. In this paper, for real noisy image denoising, we propose a multi-channel WNNM model which preserve the power of WNNM and be able to process the differences among different channels.

135

### 2.2. Real Color Image Denoising

136

During the last decade, several denoising methods are proposed for real color image denoising [15–17, 19]. Among them, the CBM3D [15] first transform the RGB image into luminance-chrominance space (e.g., YCbCr) and then apply the famous BM3D method [2] on each channel separately with the patches being grouped only in the luminance channel. In [16], the authors proposed the “Noise Level Function” to estimate and remove the noise for each channel in natural images. However, the methods processing each channel separately would achieve inferior performance than processing jointly these channels [14]. The methods of [17, 19, 25] perform real color image denoising by concatenating the patches in R, G, B channels into joint vectors. However, the concatenation would treat each channel equally and ignore the different noise properties among these channels. The method in [18] models the cross-channel noise in real noisy image as a multivariate Gaussian and the noise is removed by the Bayesian non-local means filter [26]. The commercial software Neat Image [27] estimates the noise parameters from a flat region of the given noisy image and filters the noise correspondingly. But these methods [18, 27] ignore the non-local self similarity property of natural images [2, 7].

160

In this paper, we introduce a weighting matrix which add different weights to different channels for color image

denoising. The proposed multi-channel method can effectively solve the problem of different noise structures among different channels.

162

163

164

165

166

167

168

169

170

171

172

173

174

175

176

177

178

179

180

181

182

183

184

185

186

187

188

189

190

191

192

193

194

195

196

197

198

199

200

201

202

203

204

205

206

207

208

209

210

211

212

213

214

215

## 3. Color Image Denoising via Multi-channel Weighted Nuclear Norm Minimization

### 3.1. The Problem

The color image denoising problem can be formulated as follows: given a color image with Red (R), Green (G), Blue (B) channels, each channel is degraded by some certain synthetic or real noise and we aim to recover the clean image from its degraded version. The noise structures in each channel are different due to the on-board processing of the in-camera imaging pipeline [13]. Therefore, it is problematic to directly apply denoising methods to the joint vectors concatenated by corresponding patches of the R, G, B channels. To validate this point, in Fig. 1, we show the clean image “kodim23” taken from the Kodak PhotoCD dataset, its degraded version generated by adding synthetic additive white Gaussian noise (AWGN) to each channel of “kodim23”, and the denoised image by applying WNNM [7] on the joint vectors concatenated from R, G, B channels of the degraded image. The standard derivations of AWGN added to the R, G, B channels are  $\sigma_r = 40$ ,  $\sigma_g = 20$ ,  $\sigma_b = 30$ , respectively. The input standard derivation of the noise for the concatenated WNNM method is set as the Root Mean Square (RMS) of those in each channel, i.e.,  $\sigma = \sqrt{(\sigma_r^2 + \sigma_g^2 + \sigma_b^2)/3} = 31.1$ . From Fig. 1, one can see that the concatenated WNNM method treating each channel equally would remain some noise in the R and B channel, while oversmoothing the G channel of the degraded image. Hence, if the patches of different channels are treated adaptively in the concatenated vectors, the degraded color images would be recovered with better visual qualities.

In order to process each channel differently while still exploiting the joint structures of the color images, in this paper, we introduce a weighting matrix  $\mathbf{W}$  to the concatenated WNNM method. Assume the matrix  $\mathbf{Y}$  containing the noisy patches in R, G, B channels as  $\mathbf{Y} = [\mathbf{Y}_r^\top \mathbf{Y}_g^\top \mathbf{Y}_b^\top]^\top$ , the corresponding clean matrix  $\mathbf{X} = [\mathbf{X}_r^\top \mathbf{X}_g^\top \mathbf{X}_b^\top]^\top$ , and the weights  $w$  for the singular values of  $\mathbf{X}$ , then the proposed multi-channel WNNM model is

$$\min_{\mathbf{X}} \|\mathbf{W}(\mathbf{Y} - \mathbf{X})\|_F^2 + \|\mathbf{X}\|_{w,*} \quad (4)$$

The setting of the weighting matrix  $\mathbf{W}$  and the algorithm solving this model will be introduced as follows.

### 3.2. The Setting of Weighting Matrix $\mathbf{W}$

For simplicity, in this paper, we assume the weighting matrix  $\mathbf{W}$  to be diagonal, which can process different channels with different weights. The setting of the weights in

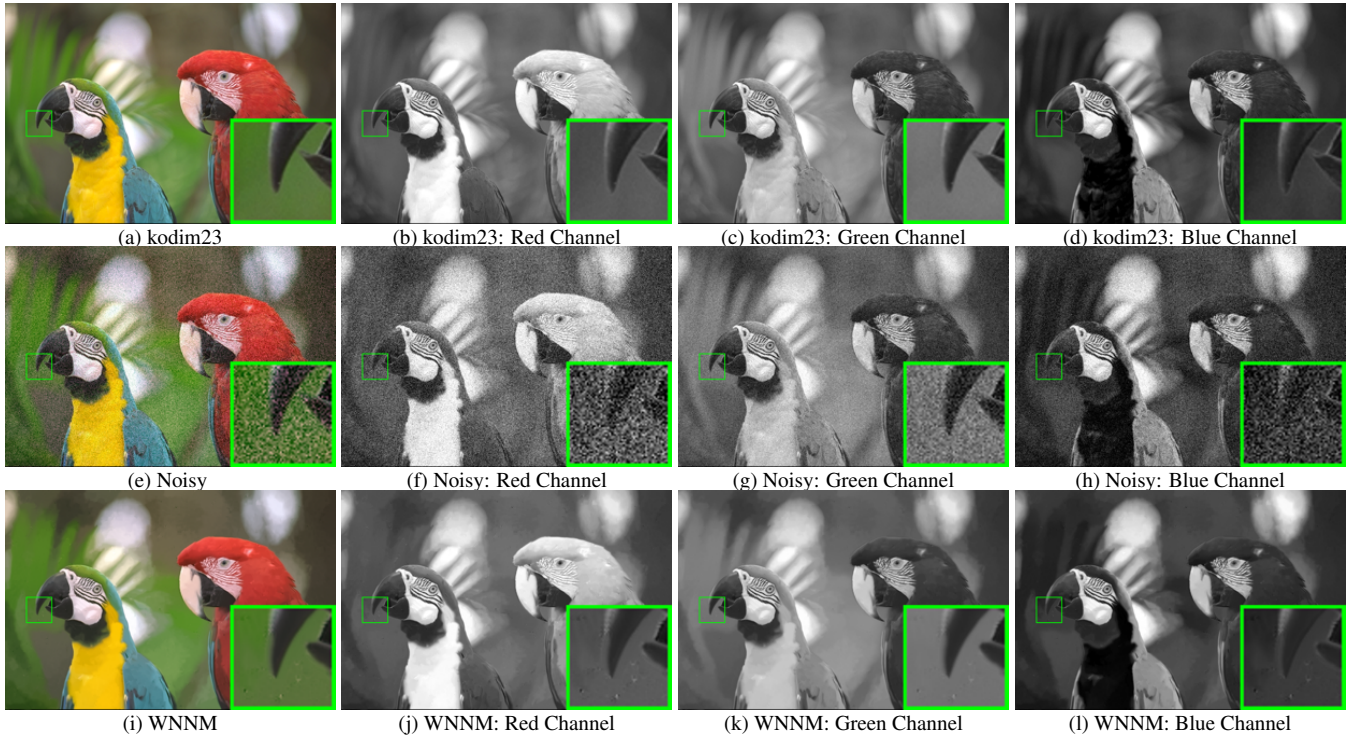


Figure 1. The image “kodim23” of the Kodak PhotoCD dataset, its degraded version, and the image recovered by WNNM. The R, G, B channels are also listed here for image quality comparison.

the weighting matrix  $\mathbf{W}$  can be automatically determined under the Bayesian framework:

$$\begin{aligned} \hat{\mathbf{X}} &= \arg \max_{\mathbf{X}} \ln P(\mathbf{X}|\mathbf{Y}, \mathbf{w}) \\ &= \arg \max_{\mathbf{X}} \{\ln P(\mathbf{Y}|\mathbf{X}) + \ln P(\mathbf{X}|\mathbf{w})\}. \end{aligned} \quad (5)$$

The log-likelihood term  $\ln P(\mathbf{Y}|\mathbf{X})$  is characterized by the statistics of noise, which is assumed to be channel-wise independent white Gaussian with standard deviations  $\{\sigma_r, \sigma_g, \sigma_b\}$

$$P(\mathbf{Y}|\mathbf{X}) = \prod_{c \in \{r, g, b\}} (2\pi\sigma_c^2)^{-\frac{3p^2}{2}} \exp\left(-\frac{1}{2\sigma_c^2} \|\mathbf{Y}_c - \mathbf{X}_c\|_F^2\right).$$

We assume that the matrix  $\mathbf{X}$  follows the following distribution

$$P(\mathbf{X}|\mathbf{w}) \propto \exp\left(-\frac{1}{2} \|\mathbf{X}\|_{\mathbf{w}, *}\right). \quad (6)$$

Putting (8) and (7) into (6), we have

$$\hat{\mathbf{X}} = \arg \min_{\mathbf{X}} \|\mathbf{W}(\mathbf{Y} - \mathbf{X})\|_F^2 + \|\mathbf{X}\|_{\mathbf{w}, *}, \quad (8)$$

where

$$\mathbf{W} = \begin{pmatrix} \sigma_r^{-2} \mathbf{I} & \mathbf{0} & \mathbf{0} \\ \mathbf{0} & \sigma_g^{-2} \mathbf{I} & \mathbf{0} \\ \mathbf{0} & \mathbf{0} & \sigma_b^{-2} \mathbf{I} \end{pmatrix}. \quad (9)$$

### 3.3. The Denoising Algorithm

In this section, we apply the proposed multi-channel WNNM model on color image denoising problem. The multi-channel WNNM model can make use of the non-local self similarity property of natural images while treating each channel adaptively. In real-world noisy images, the

noise are first emerged in the RAW data, i.e., color filter array (CFA). The major noise generated in real noisy images are due to the discrete nature of light and thermal agitation [], which can be modeled as Poisson and Gaussian distribution, respectively. Since the Poisson distribution can be approximately modeled by Gaussian distribution, the overall noise model in each channel of the color image could be Gaussian. Hence, in this work we still choose to deal with the RGB channels in color images. Besides, even though if the demosaicing of RAW image generate similar distribution in noise in different channels, the channel-wise scaling in white balance would definitely change the noise distribution in each channel. Thus, the noise in R, G, B channels are definitely different which can be described by different noise levels and structures. According to above analysis, color image denoising is to recover the latent clean image  $\mathbf{x}$  from the observed noisy version  $\mathbf{y}_c = \mathbf{x}_c + \mathbf{n}_c$ , where  $c \in \{R, G, B\}$  represent the R, G, B channels in color images and  $\mathbf{n}_c$  is the noise in the  $c$  channel (assumed to be additive white Gaussian noise).

The patches in color image  $\mathbf{y}$  are of size  $p \times p \times 3$ . For each patch  $\mathbf{y}_j$ , we search its non-local similar patches in a large area and stack the similar patches column by column. The resulting matrix  $\mathbf{Y}_j \in \mathbb{R}^{3p^2 \times n}$ , where  $n$  is the number of similar patches. The corresponding matrices containing the clean patches and the channel-wise noise are defined as  $\mathbf{X}_j$  and  $\mathbf{N}_j$ , respectively. Since  $\mathbf{X}_j$  is made of simi-

270  
271  
272  
273  
274  
275  
276  
277  
278  
279  
280  
281  
282  
283  
284  
285  
286  
287  
288  
289  
290  
291  
292  
293  
294  
295  
296  
297  
298  
299  
300  
301  
302  
303  
304  
305  
306  
307  
308  
309  
310  
311  
312  
313  
314  
315  
316  
317  
318  
319  
320  
321  
322  
323

324 **A2: Color Image Denoising by Multi-channel WNNM**  
 325 **Input:** Noisy image  $\mathbf{y}$ , noise levels  $\{\sigma_r, \sigma_g, \sigma_b\}$ ;  
 326 **Initialization:**  $\hat{\mathbf{x}}^{(0)} = \mathbf{y}, \mathbf{y}^{(0)} = \mathbf{y}$ ;  
 327 **for**  $k = 1 : K_2$  **do**  
 328   1. Set  $\mathbf{y}^{(k)} = \hat{\mathbf{x}}^{(k-1)}$ ;  
 329   2. Extracte local patches  $\{\mathbf{y}_j\}_{j=1}^N$  from  $\mathbf{y}^{(k)}$ ;  
 330     **for** each patch  $\mathbf{y}_j$  **do**  
 331       3. Search non-local similar patches  $\mathbf{Y}_j$ ;  
 332       4. Estimate  $\mathbf{X}_j$  by applying the Algorithm 1 to  $\mathbf{Y}_j$ ;  
 333     **end for**  
 334   5. Aggregate  $\{\mathbf{X}_j\}_{j=1}^N$  to form the image  $\hat{\mathbf{x}}^{(k)}$ ;  
 335   **end for**  
 336   **Output:** Denoised image  $\hat{\mathbf{x}}^{K_2}$ .

338  
 339 lar patches, it should be a low rank matrix. And hence the  
 340 multi-channel WNNM model proposed in this paper can be  
 341 used here. Compared to the original single channel WNNM  
 342 model [7] proposed for grayscale image denoising  
 343

$$\min_{\mathbf{X}_j} \|\mathbf{W}_j(\mathbf{Y}_j - \mathbf{X}_j)\|_F^2 + \|\mathbf{X}_j\|_{w,*}. \quad (10)$$

344 When the weighting matrix  $\mathbf{W}_j = \frac{1}{\sigma_n^2} \mathbf{I}$ , where  $\mathbf{I} \in$   
 345  $\mathbb{R}^{3p^2 \times 3p^2}$  is the identity matrix, the multi-channel WNNM  
 346 model will reduce to the WNNM model as a special case.  
 347 The design of WNNM model also motivate us to consider  
 348 a similar design of the weighting matrix. In order to deal  
 349 with color image denoising task, the weighting matrix  $\mathbf{W}_j$   
 350 should be modified to be suitable for multi-channel cases.  
 351 In fact, for the color image denoising task, a holistic try of  
 352 the weighting matrix  $\mathbf{W}_j$  could be  
 353

354 Here, for simplicity, we assume that the noise in different  
 355 channels are independent to each other. The experimental  
 356 results have already demonstrated that this simple  
 357 assumption could already generate the best denoising  
 358 performance on benchmark real noisy image dataset. In this  
 359 paper, we did not consider the correlations of noise among  
 360 different channels, which is the future work of our research  
 361 line. The determination of the weight vector in weighted  
 362 nuclear norm is the same as in the WNNM model [23]. We  
 363 set the weight vector as  $w_i^{k+1} = \frac{C}{|\sigma_i(\mathbf{X}_k)| + \epsilon}$ .  
 364

365 The multi-channel WNNM is applied to the non-local  
 366 similar patches of each local patch in the noisy image  $\mathbf{y}$ .  
 367 And then all the patches are aggregated together to form the  
 368 final recovered image  $\hat{\mathbf{y}}$ . We also perform the denoising  
 369 procedure for several ( $K_2$ ) iterations to obtain better  
 370 denoising results. In Algorithm 2 (A2), we summarizes the  
 371 denoising steps of multi-channel WNNM model on color  
 372 image denoising.

### 374 3.4. Optimization

375 Unfortunately, the proposed multi-channel WNNM  
 376 problem cannot be solved in an analytical form. In [23],

377 when the weights on singular values are non-descending,  
 378 the weighted nuclear norm proximal operator can have  
 379 global optimum with closed-form solution. However, such  
 380 property is not valid for the multi-channel WNNM model.  
 381 The reason is that the weighting matrix  $\mathbf{W}$  is added to the  
 382 matrix  $\mathbf{X}$  instead of its singular values. Besides, the ele-  
 383 ments in  $\mathbf{W}$  is not in a non-descending order with respect  
 384 to the singular value of  $\mathbf{X}$ . This makes the proposed model  
 385 more difficult to optimize than the original WNNM model.  
 386

387 This can be solved by introducing an augmented variable  
 388  $\mathbf{Z}$ , and the above multi-channel WNNM problem is equiva-  
 389 lent to a linearly constrained non-convex problem with two  
 390 variables.

$$\min_{\mathbf{X}, \mathbf{Z}} \|\mathbf{W}(\mathbf{Y} - \mathbf{X})\|_F^2 + \|\mathbf{Z}\|_{w,*} \quad \text{s.t.} \quad \mathbf{X} = \mathbf{Z}. \quad (11)$$

392 This is an optimization problem with functions of two vari-  
 393 ables  $\mathbf{X}$  and  $\mathbf{Z}$  with linearly constrained condition of  $\mathbf{X} =$   
 394  $\mathbf{Z}$ . In fact, this proplem can be solved by the alternating  
 395 direction method of multipliers (ADMM) algorithm.

396 To solve the above optimization problem, we first derive  
 397 its augmented Lagrangian function as

$$\begin{aligned} \mathcal{L}(\mathbf{X}, \mathbf{Z}, \mathbf{A}, \rho) = & \|\mathbf{W}(\mathbf{Y} - \mathbf{X})\|_F^2 + \|\mathbf{Z}\|_{w,*} \\ & + \langle \mathbf{A}, \mathbf{X} - \mathbf{Z} \rangle + \frac{\rho}{2} \|\mathbf{X} - \mathbf{Z}\|_F^2 \end{aligned} \quad (12)$$

400 where  $\mathbf{A}$  is the augmented Lagrangian multiplier and  $\rho > 0$   
 401 is the penalty parameter.

402 We initialize the matrix variables  $\mathbf{X}_0$ ,  $\mathbf{Z}_0$ , and  $\mathbf{A}_0$  to be  
 403 zero matrix of suitable size. Taking derivative of the La-  
 404 grangian function  $\mathcal{L}$  with respect to the variables  $\mathbf{X}$  and  $\mathbf{Z}$   
 405 and setting the derivative function to be zero, we can alter-  
 406 natively update the iterations of the ADMM algorithm as  
 407 follows:

408 (1) Update  $\mathbf{X}$  while fixing  $\mathbf{Z}$  and  $\mathbf{A}$ :

$$\mathbf{X}_{k+1} = \arg \min_{\mathbf{X}} \|\mathbf{WY} - \mathbf{WX}\|_F^2 + \frac{\rho_k}{2} \|\mathbf{X} - \mathbf{Z}_k + \rho_k^{-1} \mathbf{A}_k\|_F^2 \quad (13)$$

411 This is a mixed weighted least square and standard least  
 412 square problem and we could derive its closed-form solu-  
 413 tion:

$$\mathbf{X}_{k+1} = (\mathbf{W}^\top \mathbf{W} + \frac{\rho_k}{2} \mathbf{I})^{-1} (\mathbf{W}^\top \mathbf{WY} + \frac{\rho_k}{2} \mathbf{Z}_k - \frac{1}{2} \mathbf{A}_k) \quad (14)$$

423 (2) Update  $\mathbf{Z}$  while fixing  $\mathbf{X}$  and  $\mathbf{A}$ :

$$\mathbf{Z}_{k+1} = \arg \min_{\mathbf{Z}} \frac{\rho_k}{2} \|\mathbf{Z} - (\mathbf{X}_{k+1} + \rho_k^{-1} \mathbf{A}_k)\|_F^2 + \|\mathbf{Z}\|_{w,*} \quad (15)$$

428 According to the Theorem 1 in [23], given the  $\mathbf{X}_{k+1} +$   
 429  $\rho_k^{-1} \mathbf{A}_k = \mathbf{U}_k \Sigma_k \mathbf{V}_k^\top$  be the SVD of  $\mathbf{X}_{k+1} + \rho_k^{-1} \mathbf{A}_k$ ,  
 430 where  $\Sigma_k = \begin{pmatrix} \text{diag}(\sigma_1, \sigma_2, \dots, \sigma_n) \\ \mathbf{0} \end{pmatrix} \in \mathbb{R}^{m \times n}$ , then the

global optimum of the above problem is  $\hat{\mathbf{Z}} = \mathbf{U}_k \hat{\Sigma}_k \mathbf{V}_k^\top$ , where  $\hat{\Sigma}_k = \begin{pmatrix} \text{diag}(\hat{\sigma}_1, \hat{\sigma}_2, \dots, \hat{\sigma}_n) \\ 0 \end{pmatrix} \in \mathbb{R}^{m \times n}$  and  $(\hat{\sigma}_1, \hat{\sigma}_2, \dots, \hat{\sigma}_n)$  is the solution to the following convex optimization problem:

$$\begin{aligned} & \min_{\hat{\sigma}_1, \hat{\sigma}_2, \dots, \hat{\sigma}_n} \sum_{i=1}^n (\sigma_i - \hat{\sigma}_i)^2 + \frac{2w_i}{\rho_k} \hat{\sigma}_i \\ & \text{s.t. } \hat{\sigma}_1 \geq \hat{\sigma}_2 \geq \dots \geq \hat{\sigma}_n \geq 0. \end{aligned} \quad (16)$$

According to the Remark 1 in [23], the problem above has closed-form solution

$$\hat{\sigma}_i = \begin{cases} 0 & \text{if } c_2 < 0 \\ \frac{c_1 + \sqrt{c_2}}{2} & \text{if } c_2 \geq 0 \end{cases} \quad (17)$$

where  $c_1 = \sigma_i - \epsilon$ ,  $c_2 = (\sigma_i - \epsilon)^2 - \frac{8C}{\rho_k}$  and  $C$  is set as  $\sqrt{2n}$  by experience in image denoising.

(3) Update  $\mathbf{A}$  while fixing  $\mathbf{X}$  and  $\mathbf{Z}$ :

$$\mathbf{A}_{k+1} = \mathbf{A}_k + \rho_k (\mathbf{X}_{k+1} - \mathbf{Z}_{k+1}) \quad (18)$$

(4) Update  $\rho_k$  as  $\rho_{k+1} = \mu * \rho_k$ , where  $\mu > 1$  is a .

The above 4 alternative updating steps are repeated until the convergence conditions are satisfied or the number of iterations exceeds a preset maximum number, e.g.,  $K_1$ . The overall algorithm will achieve its convergence conditions when  $\|\mathbf{X}_{k+1} - \mathbf{Z}_{k+1}\|_F \leq \text{Tol}$ ,  $\|\mathbf{X}_{k+1} - \mathbf{X}_k\|_F \leq \text{Tol}$ , and  $\|\mathbf{Z}_{k+1} - \mathbf{Z}_k\|_F \leq \text{Tol}$  are simultaneously satisfied, where  $\text{Tol} > 0$  is a small tolerance. We summarize the optimization steps in Algorithm 1 (A1). We give a theorem, i.e., Theorem 1, to guarantee the convergence of the proposed Algorithm 1. Note that since the weighted nuclear norm is non-convex in general, we employ an unbounded sequence of  $\{\rho_k\}$  here to make sure that the Algorithm 1 is convergent.

**Theorem 1.** Assume the weights in  $\mathbf{w}$  are in a non-descending order, the sequence  $\{\mathbf{X}_k\}$ ,  $\{\mathbf{Z}_k\}$ , and  $\{\mathbf{A}_k\}$  generated in Algorithm 1 satisfy:

$$(1) \lim_{k \rightarrow \infty} \|\mathbf{X}_{k+1} - \mathbf{Z}_{k+1}\|_F = 0; \quad (19)$$

$$(2) \lim_{k \rightarrow \infty} \|\mathbf{X}_{k+1} - \mathbf{X}_k\|_F = 0; \quad (20)$$

$$(3) \lim_{k \rightarrow \infty} \|\mathbf{Z}_{k+1} - \mathbf{Z}_k\|_F = 0. \quad (21)$$

*Proof.* We give proof sketch here and detailed proof of this theorem can be found in Appendix. We can first proof that the sequence  $\{\mathbf{A}_k\}$  generated by Algorithm 1 is upper bounded. Since  $\{\rho_k\}$  is unbounded, that is  $\lim_{k \rightarrow \infty} \rho_k = +\infty$ , we can proof that the sequence of Lagrangian function  $\{\mathcal{L}(\mathbf{X}_{k+1}, \mathbf{Z}_{k+1}, \mathbf{A}_k, \rho_k)\}$  is also upper bounded. Hence, both  $\{\mathbf{WY} - \mathbf{WX}_k\}$  and  $\{\mathbf{Z}_k\}$  are upper bounded. According to Eq. (18), we can proof

<b>A1:</b> Solve Multi-channel WNNM via ADMM	486
<b>Input:</b> Matrices $\mathbf{Y}$ and $\mathbf{W}$ , $\mu > 1$ , $\text{Tol} > 0$ , $K_1 > 0$ ;	487
<b>Initialization:</b> $\mathbf{X}_0 = \mathbf{Z}_0 = \mathbf{A}_0 = \mathbf{0}$ , $\rho_0 > 0$ , $T = \text{False}$ ,	488
$k = 0$ ;	489
<b>While</b> ( $T == \text{false}$ ) <b>do</b>	490
1. Update $\mathbf{X}_{k+1}$ as	491
$\mathbf{X}_{k+1} = (\mathbf{W}^\top \mathbf{W} + \frac{\rho_k}{2} \mathbf{I})^{-1} (\mathbf{W}^\top \mathbf{WY} + \frac{\rho_k}{2} \mathbf{Z}_k - \frac{1}{2} \mathbf{A}_k)$	492
2. Update $\mathbf{Z}_{k+1}$ by solving the WNNM problem	493
$\min_{\mathbf{Z}} \frac{\rho_k}{2} \ \mathbf{Z} - (\mathbf{X}_{k+1} + \rho_k^{-1} \mathbf{A}_k)\ _F^2 + \ \mathbf{Z}\ _{\mathbf{w},*}$	494
3. Update $\mathbf{A}_{k+1}$ as $\mathbf{A}_{k+1} = \mathbf{A}_k + \rho_k (\mathbf{X}_{k+1} - \mathbf{Z}_{k+1})$	495
4. Update $\rho_{k+1} = \mu * \rho_k$ ;	496
5. $k \leftarrow k + 1$ ;	497
<b>if</b> ( $\ \mathbf{X}_{k+1} - \mathbf{Z}_{k+1}\ _F / \ \mathbf{Z}_{k+1}\ _F < \text{Tol}$ ) or ( $k \geq K_1$ )	498
5. $T \leftarrow \text{True}$	499
<b>end if</b>	500
<b>end while</b>	501
<b>Output:</b> Matrices $\mathbf{X}$ and $\mathbf{Z}$ .	502

that  $\lim_{k \rightarrow \infty} \|\mathbf{X}_{k+1} - \mathbf{Z}_{k+1}\|_F = \lim_{k \rightarrow \infty} \rho_k^{-1} \|\mathbf{A}_{k+1} - \mathbf{A}_k\|_F = 0$ , and (1) is proofed. Then we can proof that  $\lim_{k \rightarrow \infty} \|\mathbf{X}_{k+1} - \mathbf{X}_k\|_F \leq \lim_{k \rightarrow \infty} \|(\mathbf{W}^\top \mathbf{W} + \frac{\rho_k}{2} \mathbf{I})^{-1} (\mathbf{W}^\top \mathbf{WY} - \mathbf{W}^\top \mathbf{WZ}_k - \frac{1}{2} \mathbf{A}_k)\|_F + \rho_k^{-1} \|\mathbf{A}_k - \mathbf{A}_{k-1}\|_F = 0$  and hence (2) is proofed. Then (3) can be proofed by checking that  $\lim_{k \rightarrow \infty} \|\mathbf{Z}_{k+1} - \mathbf{Z}_k\| \leq \lim_{k \rightarrow \infty} \|\mathbf{Z}_{k+1} - \mathbf{S}_{\mathbf{w}/\rho_{k-1}}(\mathbf{Z}_{k-1})\|_F + \|\mathbf{X}_{k+1} - \mathbf{X}_k\|_F + \rho_k^{-1} \|\mathbf{A}_{k-1} + \mathbf{A}_{k+1} - \mathbf{A}_k\|_F = 0$ , where  $\mathbf{U}_{k-1} \mathbf{\Sigma}_{k-1} \mathbf{V}_{k-1}^\top$  is the SVD of the matrix  $\mathbf{X}_k + \rho_{k-1} \mathbf{A}_{k-1}$ . The proof sketch of Theorem 1 is end.  $\square$

## 4. Experiments

We evaluate the proposed method on synthetic noisy images as well as real noisy images. The synthetic noisy images are generated by adding additive white Gaussian noise with known noise standard derivations  $\sigma_r, \sigma_g, \sigma_b$  for the R, G, B channels, respectively. We compare the proposed method with other state-of-the-art denoising algorithms including CBM3D [2, 15], MLP [10], CSF [11], WNNM [7], TNRD [12], “Noise Clinic” [17, 25], and the commercial software Neat Image [27].

In order to take fully comparison with the original WNNM method, we extended the WNNM method [23] in three directions. The first is to apply the WNNM method on each channel separately and we still call this method “WNNM”. The second is to concatenate the corresponding patches in the R, G, B channels into a joint patch and perform denoising in a joint manner. We call this method “WNNM1”. Note that both “WNNM” and “WNNM1” have closed form solutions since they are directly extended from the original WNNM. The third is to set the weighting matrix  $\mathbf{W}$  in the proposed multi-channel WNNM model as  $\mathbf{W} = \sigma_n^2 \mathbf{I}$ . This is to more clearly validate the effectiveness of the weighting matrix by reducing the multi-channel

540 WNNM model to its special case: the WNNM model solved  
 541 by ADMM algorithm. We call this method “WNNM2”. We  
 542 set the same parameters settings for the “WNNM2” method  
 543 and the proposed multi-channel WNNM method (called  
 544 “Proposed”). For fair comparison, for “WNNM”, the cor-  
 545 responding noise levels  $\sigma_c$  of the  $c$  ( $c = r, g, b$ ) channel  
 546 is input as known parameter; for “WNNM1”, we input the  
 547 noise level as  $\sigma = \sqrt{(\sigma_r^2 + \sigma_g^2 + \sigma_b^2)/3}$  and tune the other  
 548 parameters to achieve its best denoising performance (i.e.,  
 549 highest average PSNR results); for “WNNM2”, we employ  
 550 the same parameter settings as the proposed multi-channel  
 551 WNNM method, which will be introduced in details in the  
 552 following sections.  
 553

#### 4.1. Experiments on Synthetic Noisy Images

556 In this section, we compare the proposed method with  
 557 other competing method [7, 10–12, 15, 17, 27] on 24 high  
 558 quality color images from the Kodak PhotoCD Dataset  
 559 (<http://r0k.us/graphics/kodak/>), which are  
 560 shown in Fig. 1. Then we add additive white Gaussian  
 561 noise with different standard deviations to different chan-  
 562 nels of the color images. The standard deviations of noise  
 563 we add to the R, G, B channels of the 24 clean images are  
 564 40, 20, 30, respectively. We set the patch size as  $p = 6$ , the  
 565 number of non-local similar patches as  $n = 70$ , the win-  
 566 dows size for searching similar patches as  $W = 20$ . For  
 567 the proposed multi-channel WNNM model, we set the reg-  
 568 ularization parameter as  $\lambda = 4$ , the penalty parameter as  
 569  $\rho = 6$ , the  $\mu = 1.1$ , the number of iterations in Algorithm  
 570 1 as  $K_1 = 10$ , the number of iterations in Algorithm 2 as  
 571  $K_2 = 8$ .

572 We perform quantitative comparison on the 24 high qual-  
 573 ity images from the Kodak PhotoCD Dataset, which are  
 574 widely used for color image denoising task. The PSNR re-  
 575 sults of CBM3D [2], MLP [10], TNRD [12], NC [17, 25],  
 576 NI [27], “WNNMCW” [23], “WNNMJ”, “WNNMJadmm”  
 577 and the proposed multi-channel WNNM methods are listed  
 578 in Table 1. The best PSNR results of each image are  
 579 highlighted in bold. One can see that on all the 24 im-  
 580 ages, our method achieves the best PSNR values. On  
 581 average, our proposed method has 0.45dB PSNR im-  
 582 provements over the second best method, i.e., “WNNMJ” and  
 583 much higher PSNR gains over other competing methods.  
 584 Fig. 5 shows the denoised images of a scene in the Ko-  
 585 dak PhotoCD Dataset. We can see that CBM3D, NC, and  
 586 NI would either remain noise or generate artifacts, while  
 587 MLP, TNRD “WNNMCW”, “WNNMJ”, “WNNMJadmm”  
 588 over-smooth much the image. By using the proposed multi-  
 589 channel WNNM model, our method preserves the structures  
 590 (e.g., edges and textures) better across the R, G, B channels  
 591 and generate less artifacts than other denoising methods,  
 592 leading to visually pleasant outputs. More visual compari-  
 593 ons can be found in the supplementary file.



Figure 2. The 24 high quality color images from the Kodak PhotoCD Dataset.

594  
 595  
 596  
 597  
 598  
 599  
 600  
 601  
 602  
 603  
 604  
 605  
 606  
 607  
 608  
 609  
 610  
 611  
 612  
 613  
 614  
 615  
 616  
 617  
 618  
 619  
 620  
 621  
 622  
 623  
 624  
 625  
 626  
 627  
 628  
 629  
 630  
 631  
 632  
 633  
 634  
 635  
 636  
 637  
 638  
 639  
 640  
 641  
 642  
 643  
 644  
 645  
 646  
 647

#### 4.2. Experiments on Real Noisy Images

In the second part, we compare the proposed method with other competing methods on the 15 real noisy images, , which are shown in Fig. 2, with “ground truth” clean images [18]. The noisy images were collected under controlled indoor environment. Each scene was shot 500 times under the same camera and camera setting. The mean image of the 500 shots is roughly taken as the “ground truth”, with which the PSNR can be computed. Since the image size is very large (about  $7000 \times 5000$ ) and the scenes of this dataset share repetitive contents, the authors of [18] cropped 15 smaller images (of size  $512 \times 512$ ) to perform experiments. In this section, we do not compare with the “WNNMCW” method due to its inferior performance.

We firstly perform quantitative comparison on the 15 cropped images used in [18]. The PSNR results of CBM3D [2], WNNM [7], MLP [10], TNRD [12], NC [17, 25], NI [27] and CC [18] are listed in Table 2 (The results of CC are copied from the original paper [18]). The best and second best PSNR results of each image are highlighted in red and blue, respectively. One can see that on 9 out of the 15 images, our method achieves the best PSNR values. CC achieves the best PSNR on 3 of the 15 images. It should be noted that in the CC method, a specific model is trained for each camera and camera setting, while our method uses the same model for all images. On average, our proposed method has 0.28dB PSNR improvements over [18] and much higher PSNR gains over other competing methods. Fig. 5 shows the denoised images of a scene captured by Canon 5D Mark 3 at ISO = 3200. We can see that CBM3D, WNNM, NC, NI and CC would either remain noise or generate artifacts, while MLP, TNRD over-smooth much the image. By using the proposed multi-channel WNNM model, our method preserves the structures (e.g., edges and textures) better across the R, G, B channels and generate less artifacts than other denoising methods, leading to visually pleasant outputs. More visual comparisons can be found in the supplementary file.

Table 1. PSNR(dB) results of different denoising algorithms on 20 natural images.

Image#	CBM3D	MLP	TNRD	Noise Clinic	Neat Image	WNNM	WNNM1	WNNM2	Proposed
1	25.24	25.70	25.74	24.90	23.85	26.01	25.95	25.58	26.66
2	28.27	30.12	30.21	25.87	25.90	30.08	30.11	29.80	30.20
3	28.81	31.19	31.49	28.58	26.00	31.58	31.61	31.20	32.25
4	27.95	29.88	29.86	25.67	25.82	30.13	30.16	29.84	30.49
5	25.03	26.00	26.18	25.15	24.38	26.44	26.39	25.32	26.82
6	26.24	26.84	26.90	24.74	24.65	27.39	27.30	26.88	27.98
7	27.88	30.28	30.40	27.69	25.63	30.47	30.54	29.70	30.98
8	25.05	25.59	25.83	25.30	24.02	26.71	26.75	25.26	26.90
9	28.44	30.75	30.81	27.44	25.94	30.86	30.92	30.29	31.49
10	28.27	30.38	30.57	28.42	25.87	30.65	30.68	29.95	31.26
11	26.95	28.00	28.14	24.67	25.32	28.19	28.16	27.61	28.63
12	28.76	30.87	31.05	28.37	26.01	30.97	31.06	30.58	31.48
13	23.76	23.95	23.99	22.76	23.53	24.27	24.15	23.52	24.89
14	26.02	26.97	27.11	25.68	24.94	27.20	27.15	26.55	27.57
15	28.38	30.15	30.44	28.21	26.06	30.52	30.60	30.13	30.81
16	27.75	28.82	28.87	26.66	25.69	29.27	29.21	29.02	29.96
17	27.90	29.57	29.80	28.32	25.85	29.78	29.79	29.16	30.40
18	25.77	26.40	26.41	25.70	24.74	26.63	26.56	26.01	27.22
19	27.30	28.67	28.81	26.52	25.40	29.19	29.22	28.67	29.57
20	28.96	30.40	30.76	25.90	24.95	30.79	30.83	29.97	31.07
21	26.54	27.53	27.60	26.48	25.06	27.80	27.75	27.12	28.34
22	27.05	28.17	28.27	26.60	25.36	28.21	28.16	27.81	28.64
23	29.14	32.31	32.51	23.24	26.13	31.89	31.97	31.21	32.34
24	25.75	26.41	26.53	25.73	24.55	27.10	27.03	26.18	27.59
Average	27.13	28.54	28.68	26.19	25.24	28.84	28.83	28.22	29.31

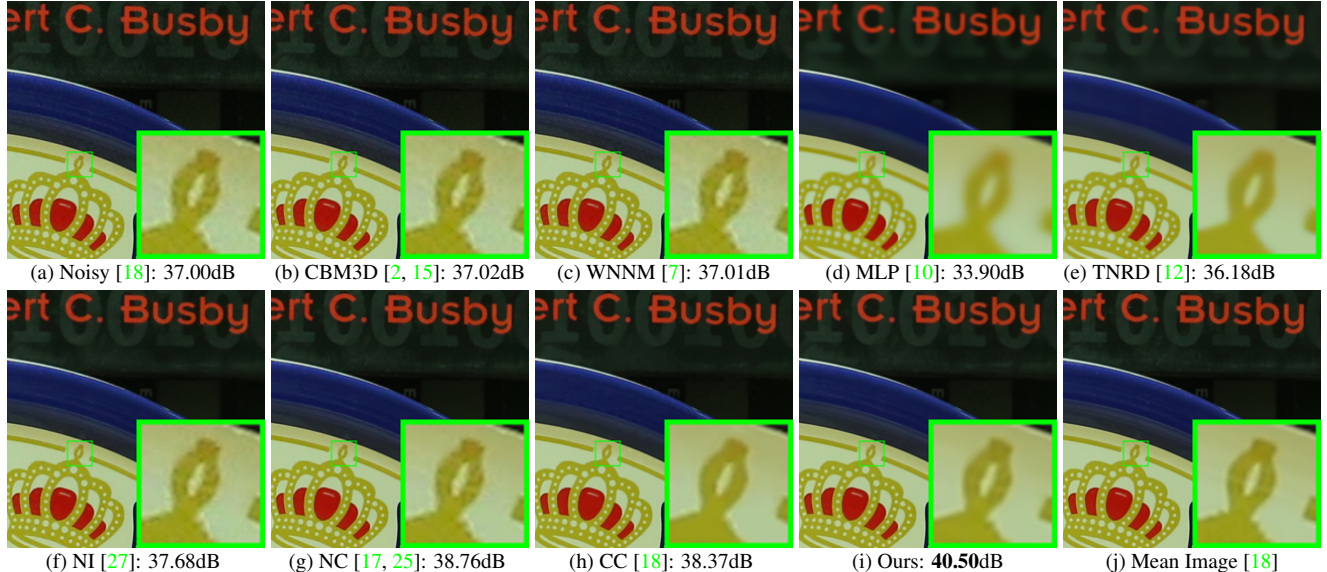


Figure 3. Denoised images of a region cropped from the real noisy image “Canon 5D Mark 3 ISO 3200 1” [18] by different methods. The images are better to be zoomed in on screen.

## 5. Conclusion and Future Work

Most existing color image denoising methods treat the R, G, B channels equally and ignore the different noise structures in different channels. Common strategies that processing each channel separately and concatenating the RGB values into joint vectors would generate false color or artifacts. In this paper, we proposed a novel model for color image denoising which can explore the different noise structures among the R, G, B channels and exploit the non-

local self similarity property of natural images. Specifically, we introduced a weighting matrix, which are employed to describe the noise levels of different channels, to the original weighted nuclear norm minimization (WNNM) model. Though the proposed model no longer has closed-form solution, we successfully solved the proposed model via the famous ADMM algorithm by introducing an additional variable with a linear constraint. The transformed problem has convergence property and can be solved in

Table 2. PSNR(dB) results of different methods on 15 cropped real noisy images used in [18].

Camera Settings	<b>CBM3D</b>	<b>MLP</b>	<b>TNRD</b>	<b>NI</b>	<b>NC</b>	<b>CC</b>	<b>WNNM1</b>	<b>WNNM2</b>	<b>Proposed</b>
Canon 5D Mark III ISO = 3200	39.76	39.00	39.51	35.68	36.20	38.37	39.74	39.98	<b>41.13</b>
	36.40	36.34	36.47	34.03	34.35	35.37	35.12	36.65	<b>37.28</b>
	36.37	36.33	36.45	32.63	33.10	34.91	33.14	34.63	<b>36.52</b>
Nikon D600 ISO = 3200	34.18	34.70	34.79	31.78	32.28	34.98	35.08	35.08	<b>35.53</b>
	35.07	36.20	36.37	35.16	35.34	35.95	36.42	36.84	<b>37.02</b>
	37.13	39.33	39.49	39.98	40.51	<b>41.15</b>	40.78	39.24	39.56
Nikon D800 ISO = 1600	36.81	37.95	38.11	34.84	35.09	37.99	38.28	38.61	<b>39.26</b>
	37.76	40.23	40.52	38.42	38.65	40.36	41.24	40.81	<b>41.43</b>
	37.51	37.94	38.17	35.79	35.85	38.30	38.04	38.96	<b>39.55</b>
Nikon D800 ISO = 3200	35.05	37.55	37.69	38.36	38.56	<b>39.01</b>	39.93	37.97	38.91
	34.07	35.91	35.90	35.53	35.76	36.75	37.32	37.30	<b>37.41</b>
	34.42	38.15	38.21	40.05	40.59	39.06	<b>41.52</b>	38.68	39.39
Nikon D800 ISO = 6400	31.13	32.69	32.81	34.08	34.25	34.61	<b>35.20</b>	34.57	34.80
	31.22	32.33	32.33	32.13	32.38	33.21	33.61	33.43	<b>33.95</b>
	30.97	32.29	32.29	31.52	31.76	33.22	33.62	34.02	<b>33.94</b>
Average	35.19	36.46	36.61	35.33	35.65	36.88	37.27	37.12	<b>37.71</b>



Figure 4. The 15 cropped real noisy images used in [18].

an alternative updating manner and both variables can be updated with closed-form solutions. We applied the proposed multi-channel WNNM model on color image denoising problem. Extensive experiments on benchmark datasets demonstrate that the proposed model outperforms the other competing denoising methods on both synthetic color noisy images as well as real-world noisy images. The introduce of the weighting matrix can indeed boost the performance of the original WNNM model on color image denoising. We believe that this work can be extended in at least three directions. Firstly, the proposed weighting matrix can be introduced into other methods designed for denoising grayscale images. Secondly, the weighting matrix beyond the diagonal form, such as correlation form [28], may bring better performance on color image denoising. Thirdly, the proposed multi-channel WNNM model can be further extended to deal with images with more channels, such as the hyperspectral images in remote sensing applications. We will focus our future work on these three directions.

## References

- [1] A. Buades, B. Coll, and J. M. Morel. A non-local algorithm for image denoising. *IEEE Conference on Computer Vision and Pattern Recognition (CVPR)*, pages 60–65, 2005. [1](#)
- [2] K. Dabov, A. Foi, V. Katkovnik, and K. Egiazarian. Image denoising by sparse 3-D transform-domain collaborative filtering. *IEEE Transactions on Image Processing*, 16(8):2080–2095, 2007. [1, 2, 5, 6, 7, 9](#)
- [3] M. Elad and M. Aharon. Image denoising via sparse and redundant representations over learned dictionaries. *IEEE Transactions on Image Processing*, 15(12):3736–3745, 2006. [841](#)
- [4] J. Mairal, F. Bach, J. Ponce, G. Sapiro, and A. Zisserman. Non-local sparse models for image restoration. *IEEE International Conference on Computer Vision (ICCV)*, pages 2272–2279, 2009. [845](#)
- [5] W. Dong, L. Zhang, G. Shi, and X. Li. Nonlocally centralized sparse representation for image restoration. *IEEE Transactions on Image Processing*, 22(4):1620–1630, 2013. [849](#)
- [6] J. Xu, L. Zhang, W. Zuo, D. Zhang, and X. Feng. Patch group based nonlocal self-similarity prior learning for image denoising. *IEEE International Conference on Computer Vision (ICCV)*, pages 244–252, 2015. [853](#)
- [7] S. Gu, L. Zhang, W. Zuo, and X. Feng. Weighted nuclear norm minimization with application to image denoising. *IEEE Conference on Computer Vision and Pattern Recognition (CVPR)*, pages 2862–2869, 2014. [1, 2, 4, 5, 6, 7, 9](#)
- [8] S. Roth and M. J. Black. Fields of experts. *International Journal of Computer Vision*, 82(2):205–229, 2009. [1](#)

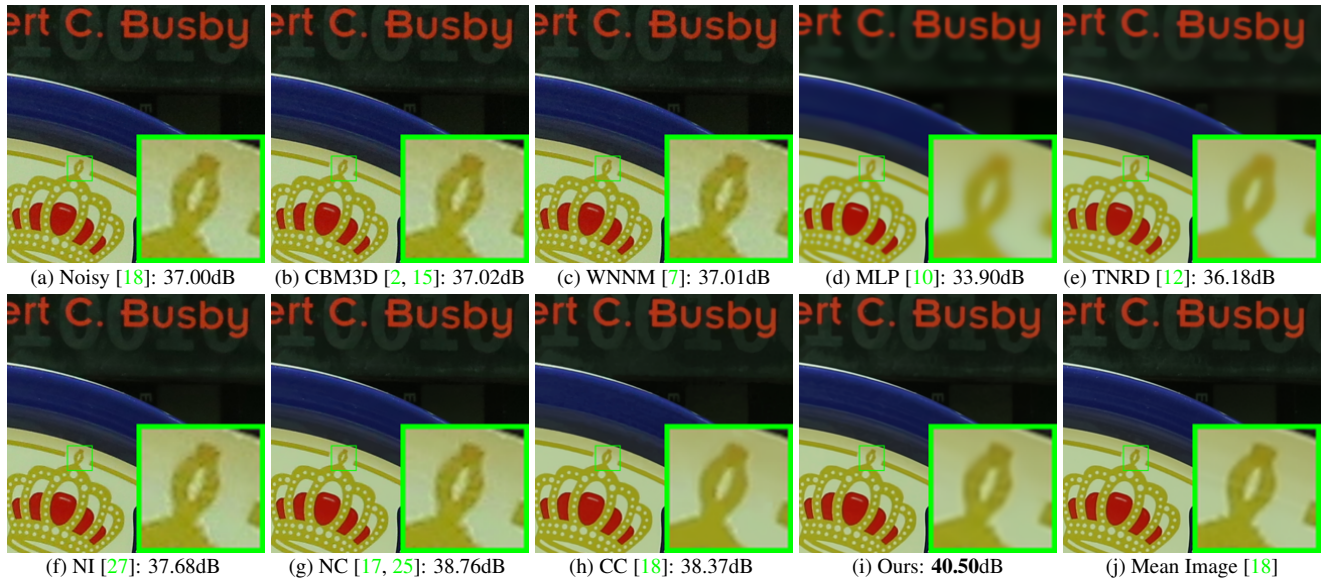


Figure 5. Denoised images of a region cropped from the real noisy image “Canon 5D Mark 3 ISO 3200 1” [18] by different methods. The images are better to be zoomed in on screen.

- [9] D. Zoran and Y. Weiss. From learning models of natural image patches to whole image restoration. *IEEE International Conference on Computer Vision (ICCV)*, pages 479–486, 2011.
- [10] H. C. Burger, C. J. Schuler, and S. Harmeling. Image denoising: Can plain neural networks compete with BM3D? *IEEE Conference on Computer Vision and Pattern Recognition (CVPR)*, pages 2392–2399, 2012. 5, 6, 7, 9
- [11] U. Schmidt and S. Roth. Shrinkage fields for effective image restoration. *IEEE Conference on Computer Vision and Pattern Recognition (CVPR)*, pages 2774–2781, June 2014. 5
- [12] Y. Chen, W. Yu, and T. Pock. On learning optimized reaction diffusion processes for effective image restoration. *IEEE Conference on Computer Vision and Pattern Recognition (CVPR)*, pages 5261–5269, 2015. 1, 5, 6, 7, 9
- [13] H. C. Karaimer and M. S. Brown. A software platform for manipulating the camera imaging pipeline. *European Conference on Computer Vision (ECCV)*, October 2016. 1, 2
- [14] Julien Mairal, Michael Elad, and Guillermo Sapiro. Sparse representation for color image restoration. *IEEE Transactions on Image Processing*, 17(1):53–69, 2008. 1, 2
- [15] K. Dabov, A. Foi, V. Katkovnik, and K. Egiazarian. Color image denoising via sparse 3D collaborative filtering with grouping constraint in luminance-chrominance space. *IEEE International Conference on Image Processing (ICIP)*, pages 313–316, 2007. 1, 2, 5, 6, 7, 9
- [16] C. Liu, R. Szeliski, S. Bing Kang, C. L. Zitnick, and W. T. Freeman. Automatic estimation and removal of noise from

a single image. *IEEE Transactions on Pattern Analysis and Machine Intelligence*, 30(2):299–314, 2008. 1, 2

- [17] M. Lebrun, M. Colom, and J.-M. Morel. Multiscale image blind denoising. *IEEE Transactions on Image Processing*, 24(10):3149–3161, 2015. 2, 5, 6, 7, 9
- [18] S. Nam, Y. Hwang, Y. Matsushita, and S. J. Kim. A holistic approach to cross-channel image noise modeling and its application to image denoising. *IEEE Conference on Computer Vision and Pattern Recognition (CVPR)*, pages 1683–1691, 2016. 1, 2, 6, 7, 8, 9
- [19] F. Zhu, G. Chen, and P.-A. Heng. From noise modeling to blind image denoising. *IEEE Conference on Computer Vision and Pattern Recognition (CVPR)*, June 2016. 1, 2
- [20] S. Boyd, N. Parikh, E. Chu, B. Peleato, and J. Eckstein. Distributed optimization and statistical learning via the alternating direction method of multipliers. *Found. Trends Mach. Learn.*, 3(1):1–122, January 2011. 1
- [21] C. Lu, C. Zhu, C. Xu, S. Yan, and Z. Lin. Generalized singular value thresholding. *AAAI*, 2015. 1
- [22] J. Cai, E. J. Candès, and Z. Shen. A singular value thresholding algorithm for matrix completion. *SIAM Journal on Optimization*, 20(4):1956–1982, 2010. 2
- [23] S. Gu, Q. Xie, D. Meng, W. Zuo, X. Feng, and L. Zhang. Weighted nuclear norm minimization and its applications to low level vision. *International Journal of Computer Vision*, pages 1–26, 2016. 2, 4, 5, 6
- [24] C. Eckart and G. Young. The approximation of one matrix by another of lower rank. *Psychometrika*, 1(3):211–218, 1936. 2

- 972 [25] M. Lebrun, M. Colom, and J. M. Morel. The noise clinic:  
973 a blind image denoising algorithm. [http://www.ipol.  
974 im/pub/art/2015/125/](http://www.ipol.im/pub/art/2015/125/). Accessed 01 28, 2015. 2, 5,  
975 6, 7, 9 1026
- 976 [26] C. Kervrann, J. Boulanger, and P. Coupé. Bayesian non-  
977 local means filter, image redundancy and adaptive dictionar-  
978 ries for noise removal. *International Conference on Scale  
979 Space and Variational Methods in Computer Vision*, pages  
980 520–532, 2007. 2 1027
- 981 [27] Neatlab ABSoft. Neat Image. [https://ni.  
982 neatvideo.com/home](https://ni.neatvideo.com/home). 2, 5, 6, 7, 9 1028
- 983 [28] N. J. Higham. Computing the nearest correlation matrix a  
984 problem from finance. *IMA Journal of Numerical Analysis*,  
985 22(3):329, 2002. 8 1029
- 986
- 987
- 988
- 989
- 990
- 991
- 992
- 993
- 994
- 995
- 996
- 997
- 998
- 999
- 1000
- 1001
- 1002
- 1003
- 1004
- 1005
- 1006
- 1007
- 1008
- 1009
- 1010
- 1011
- 1012
- 1013
- 1014
- 1015
- 1016
- 1017
- 1018
- 1019
- 1020
- 1021
- 1022
- 1023
- 1024
- 1025